LEGIBILITY NOTICE

A major purpose of the Technical Information Center is to provide the broadest dissemination possible of information contained in DOE's Research and Development Reports to business, industry, the academic community, and federal, state and local governments.

Although a small portion of this report is not reproducible, it is being made available to expedite the availability of information on the research discussed herein.
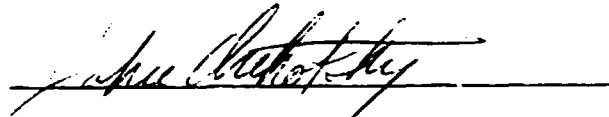
1

THIRD QUARTERLY REPORT   DOE/NBM--5007417

DOE/JPL Contract Co., 956766   DE85 007417

Electrical Research on Solar Cells and Photovoltaic Materials

This effort is being conducted persuant to an Interagency Agreement between the Department of Engineering (DOE) and the National Aeronautics and Space Administration (NASA) and in furtherance of work under Prime Contract NAS 7-918 between NASA and the California Institute of Technology.

John Orehotsky
Professor of Engineering
and Physics
Wilkes College
Wilkes-Barre, PA 18766

Project Identification - FSA Reliability and Engineering Science
Area
November 30, 1984
DRL No. 213

DISCLAIMER

INTRODUCTION

An important objective of the Flat-Plate Solar Cell Array Program is to increase the service lifetime of the photovoltaic modules used for terrestrial energy applications. The current—voltage response characteristics of the solar cells encapsulated in the modules is found to degrade with service time and this degratation places a limitation on the useful lifetime of the modules.

Corrosion appears to be one important physical mechanism that degrades the current-voltage response of the solar cells, and any effort that increases the lifetime by stopping the I-V degradation must address the question of minimizing the corrosion activity associated with the composite metallurgy, anti-reflection coating and p-n semiconductor materials that comprise a typical solar cell.

Minimizing the corrosion activity involves a consideration of both the electrochemical characteristics of the various composite materials in the cells and the ionic conductive properties of the pottant polymer used to encapsulate the cells. Consequently, the most desirable flat-plate array system would involve solar cells consisting of highly polarizable materials with similar electrochemical potentials where the cells would be encapsulated in polymers whose ionic concentrations and mobilities are negligibly small. Specifying a suitable polymer for pottant use is not an easy task since cross-linking agents, plasticizers, absorbed water and other ingredients can contribute significantly to the concentration of icns in the polymer.

Another possible mechanism limiting the service lifetime of the photo-voltaic modules is the gradual loss of the electrical insulation characteristics of the polymer pottant due to water absorption or due to polymer degradation from light or heat effects.

A systematic study of the properties of various polymer pottant materials and of the electrochemical corrosion mechanisms in solar cell materials is required for advancing the technology of terrestrial photovoltaic modules. The items of specific concern in the sponsored research activity at Wilkes College involve:

. Electrical and ionic resistivity of various polymer pottant materials when subjected to temperature, humidity, and UV irradiation.

. Water absorption kinetics and water solubility limits in various pottant polymers at selected temperatures and humidities.

. Corrosion characterization of the various metallization systems used in solar cell construction.

QUARTERLY RESULTS/SEPTEMBER TO NOVEMBER, 1984

The work activity in September, October and November, 1984 focused on:

(I)   Ion implantation and radiation damage effects in PVB and EVA.

(II) Water absorption and desorption in EVA and PVB.

(III) Corrosion effects in solar cells.

(I) Ion Implantation and Radiation Effects in PVB and EVA

Introduction

Two important concerns in the terrestrial photovoltaic energy program are the lifetime degradation of the solar cells as a result of corrosion effects, and the stability of the polymer pottant material when exposed to ionizing radiation. Both these concerns were addressed experimentally by investigating the influence of proton bombardment on the properties of PVB and EVA samples.

For corrosive action, the necessary ingredients—dissimilar materials, electrically conductive connecting paths, potential differences, and an ionically conducting electrolyte—are all inherently present in the polymer encapsulated, solar cell array modules. Except for the electrolyte, these ingredients in the molecules are not easily receptive to modification for minimizing corrosion, and any effort in corrosion control to improve reliability and service lifetime must then focus primarily on the ions in the polymer pottant electrolyte. A simple study of ionic effects in PVB and EVA polymer pottants was made by a proton bombardment experiment where the effect of proton fluence on the electrical resistivity of PVB and EVA was evaluated.

The mechanical and chemical stability of PVB and EVA to proton bombardment was also evaluated. The elastic modulus was used to monitor mechanical stability of a PVB sample as a function of proton fluence. The chemical stability of both EVA and PVB sample was determined by the amount of sample dissolved per unit time in methanol as a function of proton fluence.

4.

EXPERIMENTAL PROCEDURE

PVB and EVA samples were exposed to 100 KeV proton bombard-
ment for fluences up to 1.6 (10^{15}) /cm^2. The PVB samples employed
in this study were obtained from Monsanto, and the EVA samples
were supplied by Springborn Laboratories. The resistance of the
samples before and after irradiation wer measured by the ASTM
specified two probe, grounded ring technique.

The elastic modulus was evaluated from simple tensile
tests. The chemical inertness was determined by immersing pre-
weighted irradiated and non-irradiated samples in methanol for
forty-eight hours and then reweighing to determine the weight
percent polymer dissolved in this solvent.

RESULTS

Proton bombardment had a significant influence on the
resistivity. The resistivity of EVA as a function of fluence
is shown in Figure 1. At low fluences, proton bombardment
exposure increases the resistivity while continued bombardment
then decreases the resistivity linearly with fluence (ϕ):

$$\rho (\Omega\text{-cm}) = -2.8 (10^{-3}) \phi + 5.7 (10^{12}) \tag{1}$$

The resistivity of the PVB sample increased continuously
and linearly with fluence (Fig. 2):

$$\rho (\Omega\text{-cm}) = 2.4 (10^{-7}) \phi + 10^8 \tag{2}$$

Proton bombardment had only a very small influence if any on the
chemical reactivity of these polymers. PVB before and after
bombardment, dissolved appreciably in methanol (Fig. 3) and the
amount of dissolution appeared to be independent of the fluence.

Pre-bombarded EVA was inert in methanol. When exposed to a low
fluence, the EVA appeared to behave as a swollen gel by gaining
weight rathern than dissolving. At large fluence, the EVA dissolved
very slightly (Fig 3.)

Proton bombardment had an enormous influence on the elastic
modulus (Fig. 4) Exposure to a low fluence increased the elastic
modules by a factor of two while continued exposure to a fluence
of $2(10^{15})/cm^2$ decreased the modulus to its pre-bombarded value.

DISCUSSION

Electrical Resistivity

The movement of ions rather than the movement of electrons
is generally accepted   to be the dominant mechanism that
governs the conductivity characteristics of insulating polymers.
The conductivity (σ) and its reciprocal the resistivity (ρ)
of a typical insulating polymer is then dependent on the sum of
the movement of all positive and negative ionic species contained
in the polymer. This dependency can be expressed by an equation
that relates the reciprocal resistivity to the summed product
of the number of each ion(n), the mobility(μ) of each ion, and
the charg. (q) of each ion:

$$1/\rho = \sum_i n_i \, \mu_i \, q_i + \sum_j n_j \, \mu_j \, q_j \tag{3}$$

where the summation takes place over all i positive ions and j
negative ions in the polymer. Numerous positively charged
and negatively charged ionic species can exist in a typical

polymer. The peroxide type initiators, the cross linking agents,
the compounding agents for heat and light stability, plasticizing
agents, absorbed water, ionized polymer or monomer molecules
are all possible sources for supplying both the positive and
negative ions whose number and mobility determine the resistivity
of the polymer.

When the polymer is bombarded with protons, the implanted
protons can change the resistivity characteristics of the polymer
for several possible reasons. If the implanted protons remain
in the polymer as unreacted ions, the resistivity of the polymer
will be given by:

$$1/\rho = \mu_p n_p q_p + \sum_i n_i \mu_i q_i + \sum_j n_j \mu_j q_j \qquad (4)$$

where n_p is the concentration, μ_p the mobility and q_p
the charge of the implanted unreacted protons. A comparison
of Equations 3 and 4 shows that the resistivity of a bombarded
polymer whose implanted protons remain unreacted is expected to
be less than that of the pre-bombarded polymers, and is expected
to be inversely related to the fluence since the number of
unreacted protons is equal to the number of implanted protons
(n_I) which is directly related to the fluence:

$$1/\rho \sim n_p = n_I = k\phi \qquad (5)$$

where K is a constant.

If the implanted protons react with some of the negatively
charged ions in the polymer to form uncharged molecules, proton
bombardment will then either increase or decrease the resistivity
depending on the numbers of implanted protons and negatively
charged ions that react and lose their ionic character for
transporting current. In the limiting case where all the

implanted protons react with all the available negative ions, then

$$n_p = 0 = n_j$$

and the reciprocal resistivity would be given by

$$1/\rho = \sum_i n_i \mu_i q_i \qquad (6)$$

showing that the resistivity of the bombarded polymer would be

larger than the pre-bombarded value given by Equation 3.

Equations 3 to 6 form the basis upon which the resistivity

response (Figs. 1 and 2) of PVB and EVA to proton bombardment

can be analyzed.

For EVA at low fluence levels, the resistivity is larger than

its pre-bombardment value indicating that the implanted protons

are reacting with the negative ions, contained in the EVA to reduce

the number of intrinsic n_j negatively charged ions. The process

is suspected to continue with increasing fluence until enough

protons have been implanted to rea $\colon$ with all the negatively

charged ions. The resistivity of EVA would reach its maximum

value(given by Equation 6) as shown in Figure 1. Since all the

negatively charged ions have been reactively removed at this

fluence, subsequent bombardment would then implant protons that

remain in their unreacted ionic state. A decreasing resistivity

with continued fluence is then expected for EVA as shown in Figure

1.

While this model is quite adequate to describe qualitatively

the fluence dependence for the resistivity of EVA, the agreement

between the quantitative predictions of the model and the observed

experimental results is not as adequate. At a large fluence

where all the negative ions have been reacted, and proton c ier: re now

being implanted, the model predicts that the reciprocal resistivity

should be given by:

$$1/\rho = [n_I - n_j] \mu_P q_P + \sum_i n_i \mu_i q_i = n_P \mu_P q_P + \sum_i n_i \mu_i q_i \quad (7)$$

Since the number of implanted proton carriers is given

directly by the fluence (Eg. 5), Equation 7 becomes:

$$1/\rho = K\phi \mu_P q_P + \sum_i n_i \mu_i q_i \quad (8)$$

showing that the resistivity should decrease with increasing fluence

according to the inver e law:

$$\rho \sim \phi^{-1} \quad (9)$$

This particular expected decreasing resistivity behavior with increasing

fluence for EVA is not consistent with the experimental observations

where the resistivity decreases with increasing fluence according

to the linear relationship (Eq. 1):

$$\rho = 5.7(10^{12}) - 2.8(10^{-3})\phi$$

for fluence values greater than $10^{14}/cm^2$.

The resistivity response of PVB increases contiruously with

fluence (Fig. 2) and does not display the peaked behavior evident

in the EVA data. The implications of this continuously increasing

resistance response is that PVB, in comparison to EVA, contains

a relatively large number of negatively charged ions and that

even at a fluence of $10^{15}/cm^2$, there are not enough implanted

protons to react with all these negative ions. This comparison

has some merit because PVB typically contains about 40 $^w/o$

compounding agents-usually a plasticizer—while EVA contains

only about 10 $^w/o$ com; unding agents as a potential source of

negative ions.

While the model is in good qualitative accord with the experiemental results, the quantitative aspects of the model can be evaluated in more detail by examining the expected dependence of resistivity on the fluence and comparing the results with the experimentally observed dependence.

The expected influence of fluence on the resistivity of PVB where implanted protons are reacting with negative ions can be obtained from Equation 3 where n_j is now fluence dependent according to the relationship

$$n_j = n_{j_o} - n_I = n_{j_o} - K\phi \tag{10}$$

where n_{jo} is the number of negative ions present in the pre-bombarded sample and where n_I, the number of implanted protons, is also the number of the negative ions that have reacted with implanted protons to form molecules assuming that each of the implanted protons react with a negative ion. Using this result, the reciprocal resistivity becomes

$$1/\rho = \sum_i n_i \mu_i q_i + \sum_j [n_{j_o} - K\phi] \mu_j q_j \tag{11}$$

which shows that the resistivity should increase with fluence according to a generalized law in the form of:

$$\rho \sim [A - B\phi]^{-1} \tag{12}$$

This predicted dependency is not consistent with the experimentally observed dependencey in PVB where the resistivity increases linearly with fluence (Eg. 2):

$$\rho = 2.4(10^{-7})\phi + 10^8$$

Clearly, the models for the resistivity response with fluence in both EVA and PVB need some refinement to resolve these discrepancies between experimental observation and theoretical predictions.

The preceeding analysis for the behavior of the resistivity as a function of the fluence was based upon ionic carriers and their interaction with implanted pr :ons. The bombarding protons also introduce structural damage in the form of chain scission or cross linking into the molecular network of the polymer. The influence of this radiation induced damage on the resisitivity of a amorphously structured polymer insulating material is difficult to quantify but is suspected to be extremely small if observable at all. Chain scission and cross linking as a result of pr ton bombardment should have a measurable influence on the elastic modulus and the chemical inertness.

Chemical Inertness and Elastic Modulus

Chain scission should create a more readily dissolvable polymer where the amount of dissolution should increase with increasing fluence and scission should also decrease the elastic modulus for a polymer in proportion to the fluence. Cross linking .s expected to increase the elastic modulus and decrease the dissolution rate of the polymer in a suitable solvent.

Experimentally, proton bombardment is found to have only a very slight influence on the dissolution characteristics of EVA in methanol (Fig. 3). This slight influence appears to indicate that proton bombardment causes the EVA molecules to cross link at low fluence and then to experience chain scission at large fluence values.

Proton bombardment appears to have no systematically recognizable influence on the dissolution characteristics of PVB but does have a sizable impact on the elastic modulus. The elastic modulus data suggests that PVB molecules are cross linked at low fluence and then suffer chain scission at large fluence.

No systematic correlation is evident between the proposed structural damage and the experimental resistivity values as a function fluence in these EVA or PVB samples. Structural damage then appears to have little or no effect on the resistivity of these two amorphously structural polymers.

CONCLUSIONS

(1) A conductivity model based on intrinsic ionic current carriers and their interaction with implanted protons was found to provide a reasonable qualitative explanation of the fluence dependence for the resistivity of the proton bombarded PVB and EVA samples where the resistivity of the PVB samples was formed to increase with fluence while the resistivity of EVA first increased and then decreased with fluence.

(2) The exact form of these dependencies were not consistent with the predictions of the proposed models.

(3) Structural damage does not appear to influence the dissolution characteristics of PVA in any systematic way but has an enormous effect on the elastic modulus. The dissolution data for EVA and the modulus data for PVB suggests that structural damage caused by 100KeV bombarding protons appears to be cross linking at low fluence and chain scission at large fluence.

(4) Structural damage introduced into PVB and EVA by proton bombardment appears to have little influence on the electrical resistivity; suggesting that the observed changes in resistivity with fluence results from the implanted protons.

(5) PVB can be made a more attractive pottant material for module use by proton bombardment since the implanted protons apparently react with anions to form neutral molecules. The proton bombarded PVB then becomes a better electrical insulator and less electrolytic for supporting corrosion effects.

FUTURE WORK

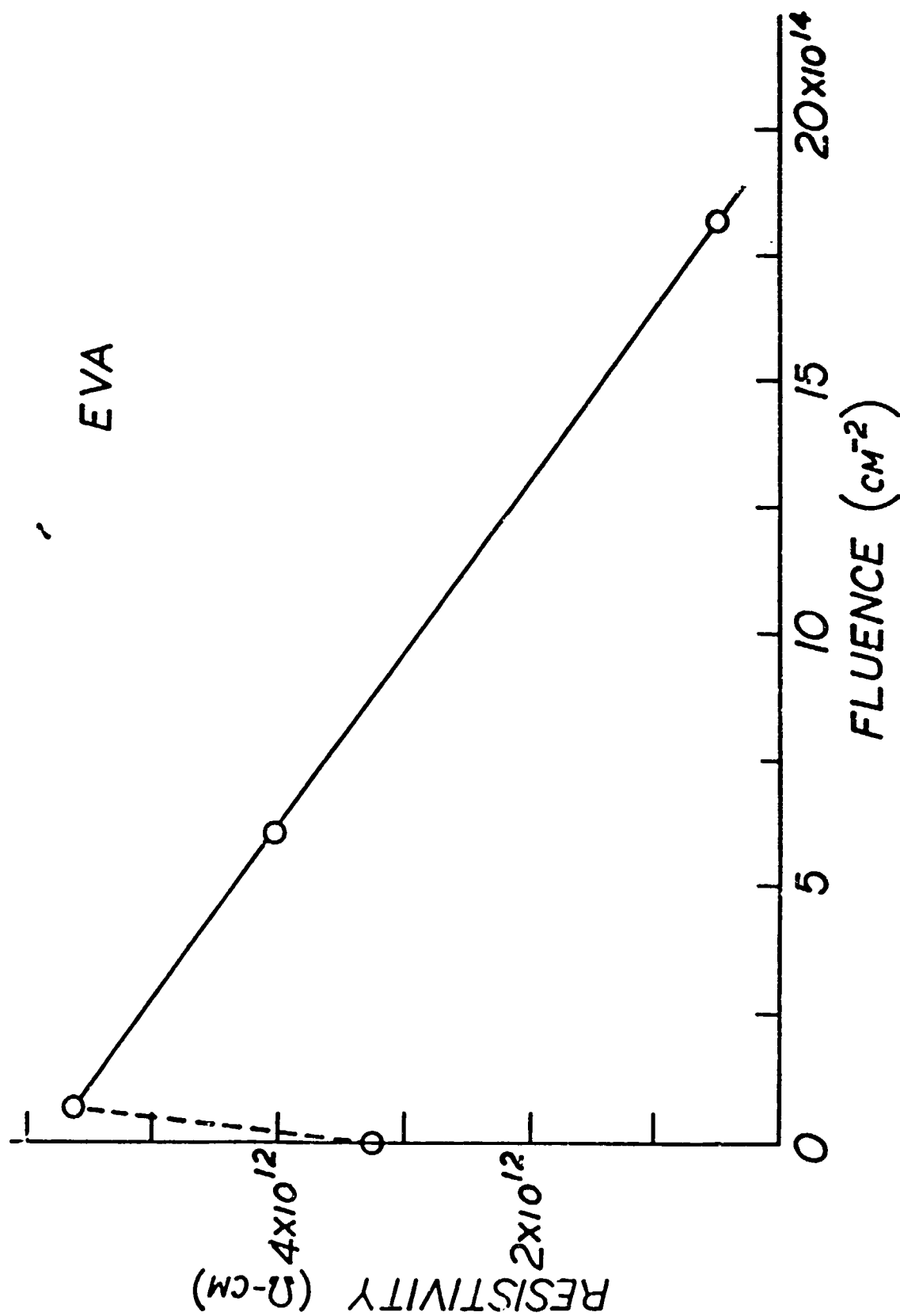No additional investigations are being planned.

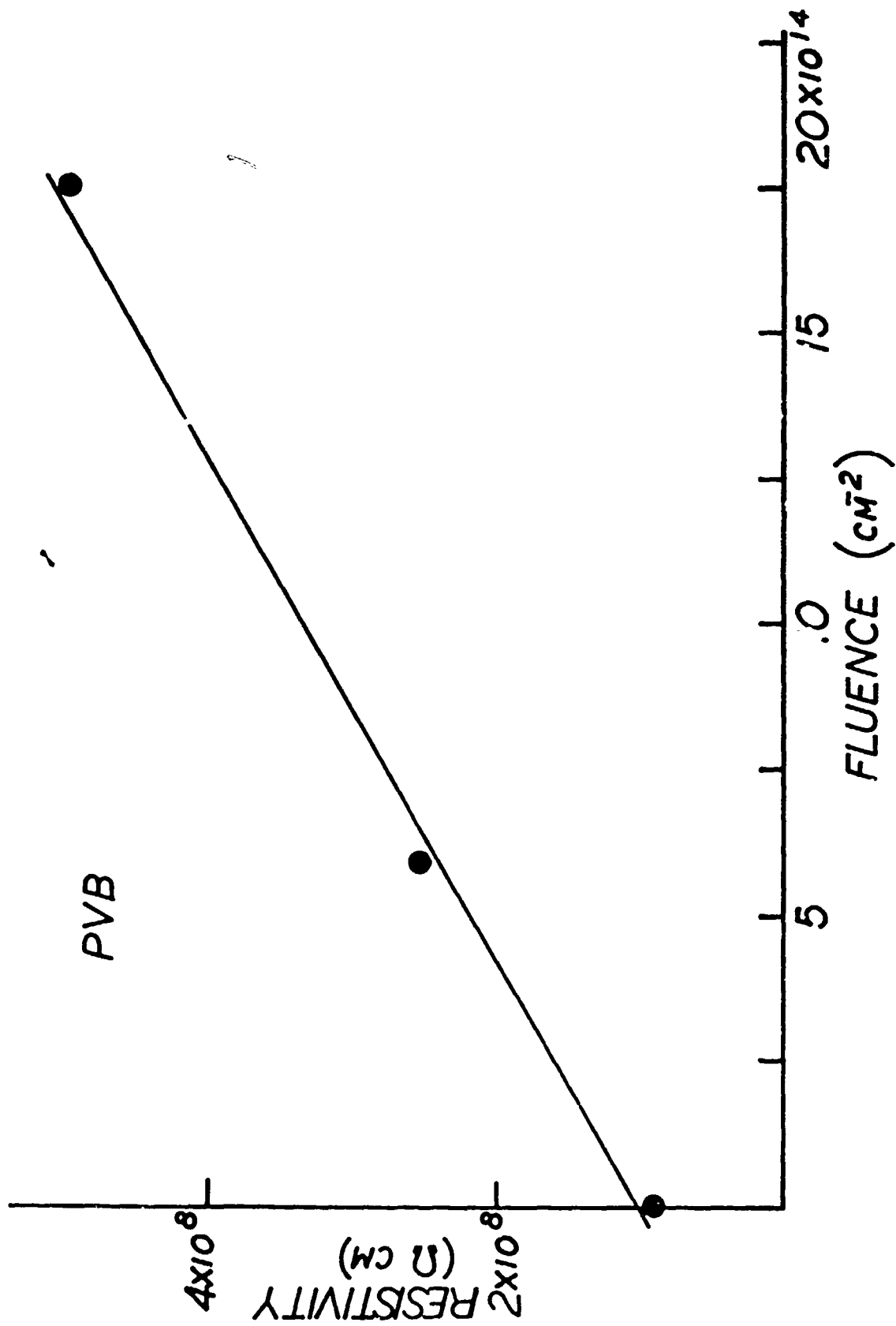Figure 1 - Resistivity of EVA as a function of proton fluence

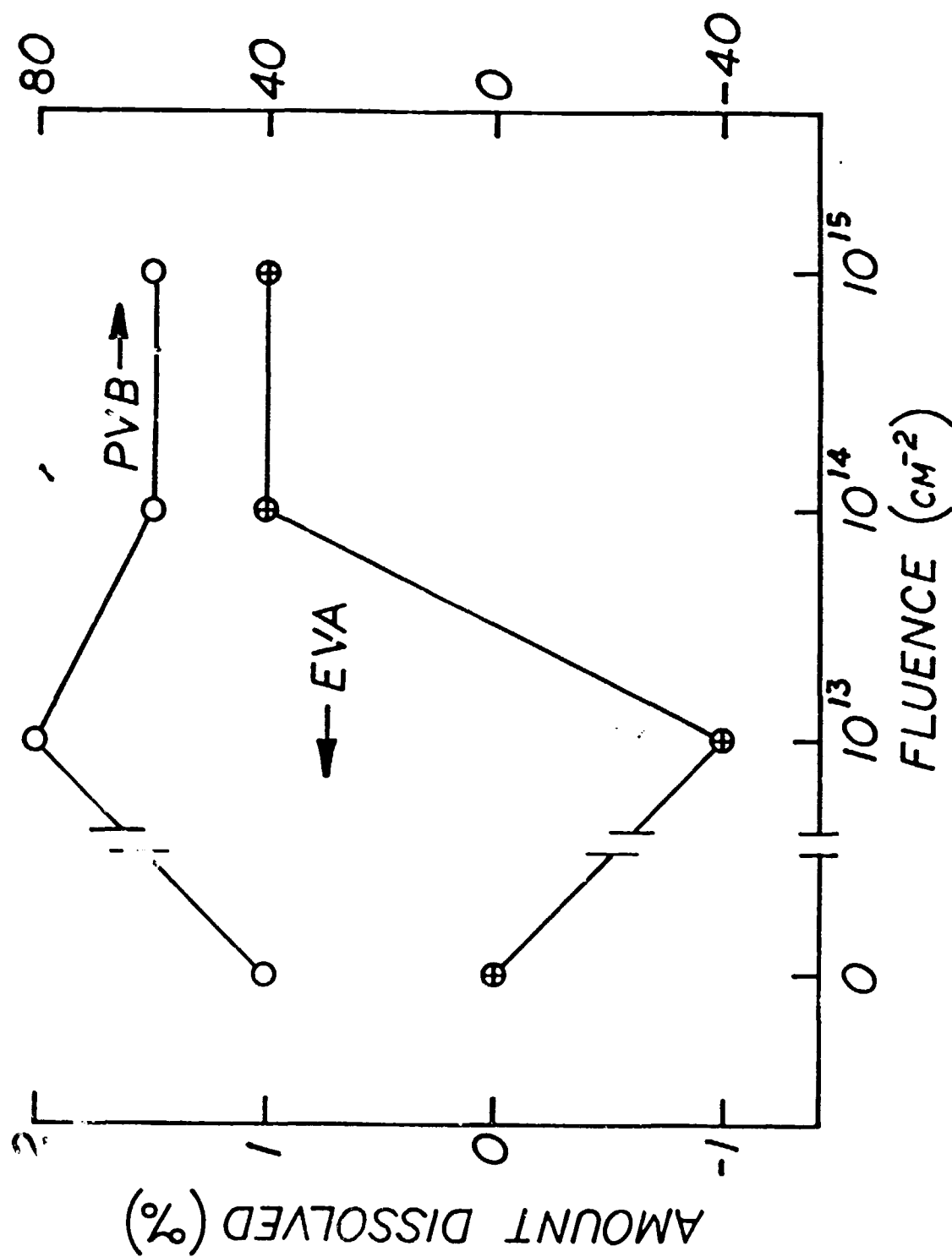Figure 2 - Resistivity of PVB as a function of proton fluence

Figure 3 – Effect of fluence on weight percent PVB and
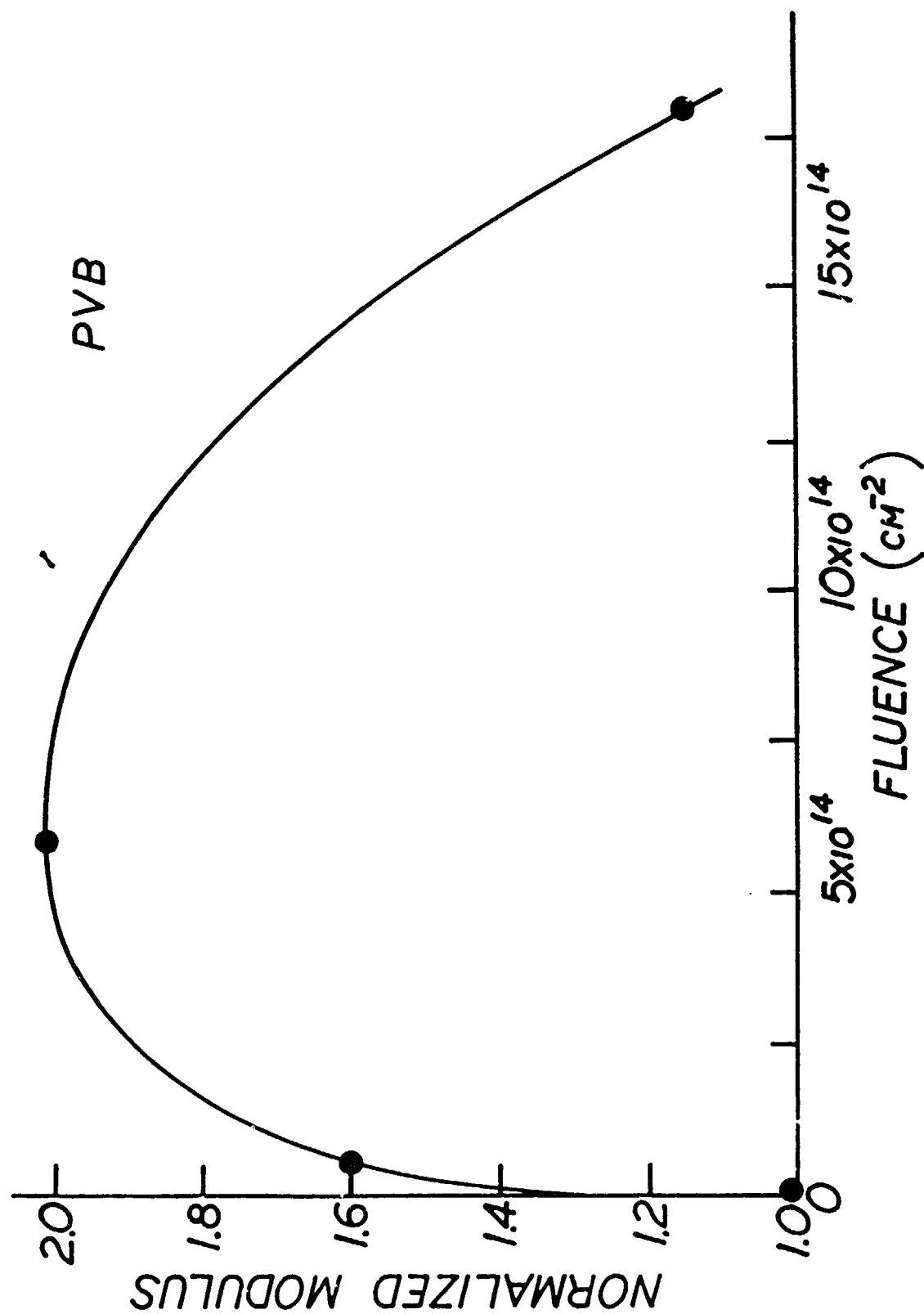EVA dissolved in methanol

Figure 4 – Normalized elastic modulus as a function of proton fluence

(II) Water Absorption and Desorption in EVA & PVB

Introduction

The two stage kinetic response characteristics observed for water absorption and desorption in EVA and PVB were suggested (Second Quarterly Report) to results from surface film effects and volume diffusion effects respectively. While the time dependent of the kinetic response and the associated activation energies appear to be supportive of the proposed two-stage model based on these effects, the value of the pre-exponential factor characterizing the volume diffusion stage in absorption is not consistent with the value obtained for the volume diffusion stage in desorption. The lack of consistency suggests that the mechanism responsible for the observed second stage kinetic response in both water absorption and desorption may be more complex than a simple volume diffusion process. A sequence of additional experiments to examine the second stage behavior in more detail were performed to help elucidate the governing mechanism. The experiment consisted of measuring the second stage absorption and desorption kinetic response in EVA and PVB samples of different thickness values. The results were compared with a square root of time/thickness dependence ($t^{\frac{1}{2}}$ / d) expected for a volume controlled diffusion mechanism in the semi-infinite plate   geometry of these samples.

Experimental

Sample thickness were .033, .066, .132, and .152 cm for PVB and .045, .094, .191, and .284 cm for EVA. The kinetics monitored gravimetrically at 53°C for water absorption and at 76°C for water desorption. The analysis consisted of correcting both the weight and time data for the first stage (surface film) effect assuming that both first and second stage behavior occur simultaneously in absorption and occur sequentially in desorption (See Second Quarterly Progress Report). The corrected data is then expected to represent second stage kinetic behavior alone without any perturbing influence from the first stage response.

Results

For water absorption, a typical plot of the second
stage normalized weight gain during water absorption as a
function of time after suitably correcting for the first
stage surface film effect is shown in Figure 1 for a 0.152
cm thick PVB sample. The corrected data display a $t^{\frac{1}{2}}$ time
dependency for the second stage behavior and this dependency
was evident in the corrected data for all the absorption and
desorption experiments in both EVA and PVB samples for the
thickness values used in these experiments.

The corrected absorption data for the PVB samples of
various thickness were plotted against $t^{\frac{1}{2}}/$ d and the results
(Fig. 2) superimpose on a linear dependency showing that the
volume diffusion mechanism is instrumental in determining
the second stage water absorption kinetic response characteris-
tics.

The water desorption data as a function of sample thickness
in the PVB samples were also corrected for first stage effects
and the second stage results, when plotted against $t^{\frac{1}{2}}$ / d
(Fig. 3), also displayed the linearity amd superposition
expected for a volume diffusion governing mechanism.

A similar corrected analysis for the second stage
water absorption and desorption response on EVA did not
display (Figs. 4 and 5) the excellent agreement in super-
position and linearity in $t^{\frac{1}{2}}$ / d that was evident in the
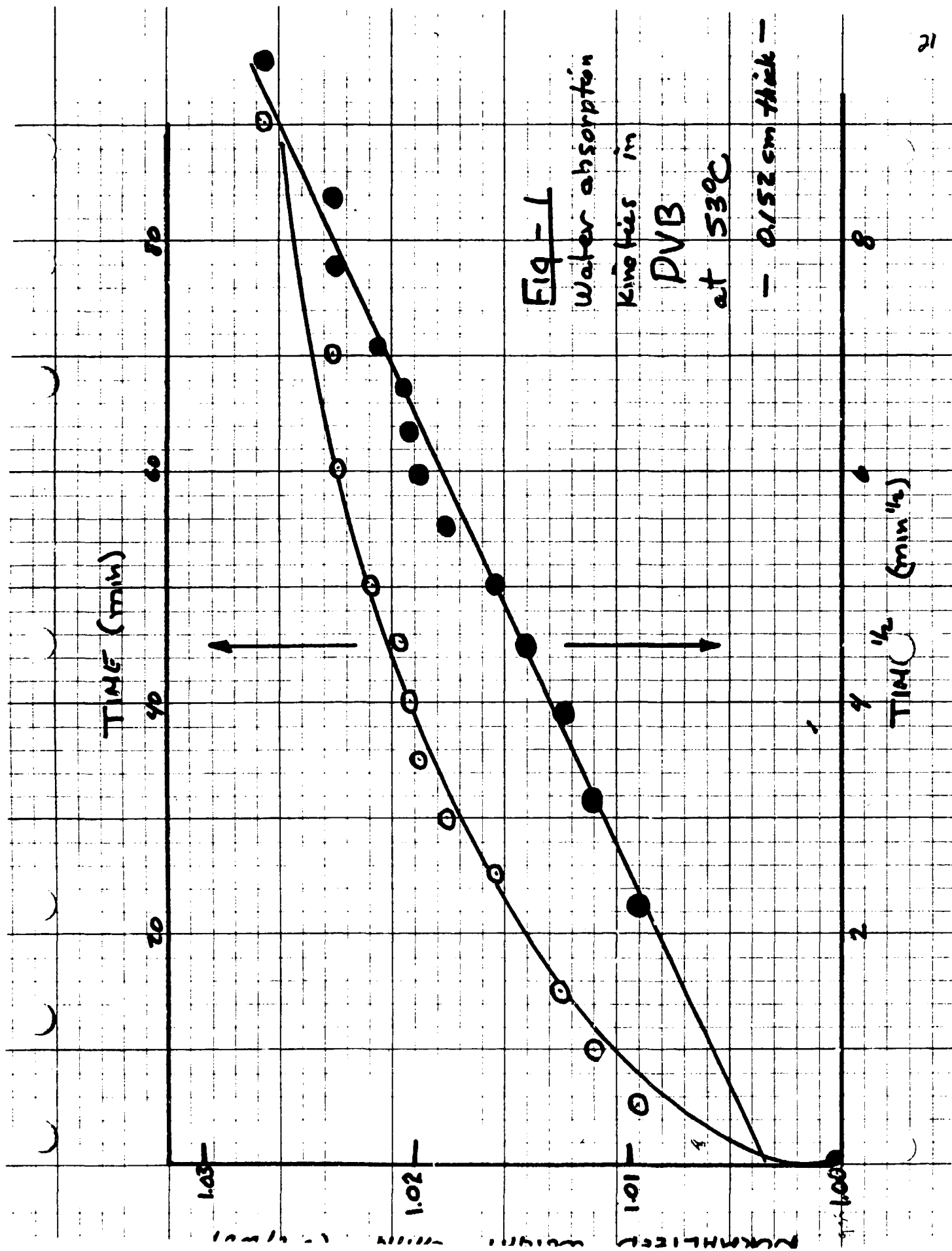PVB data. The large scatter on the EVA data does not

: .cessarily mean that volume diffusion is not the governing
mechanism for second stage behavior since the magnitude of the
weight change being monitored is quite small and the associated
errors introduced in the analysis can then become sizable.
This difficulty is not manifest in the PVB data where the
weight changes are large.

Conclusion

These experiments confirm that volume diffusion is the
governing mechanism in second stage water absorption and
desorption in PVB and probably in EVA. The water absorption
and desorption kinetics in PVB and EVA are now completed and
the results are now being prepared for possible publication.
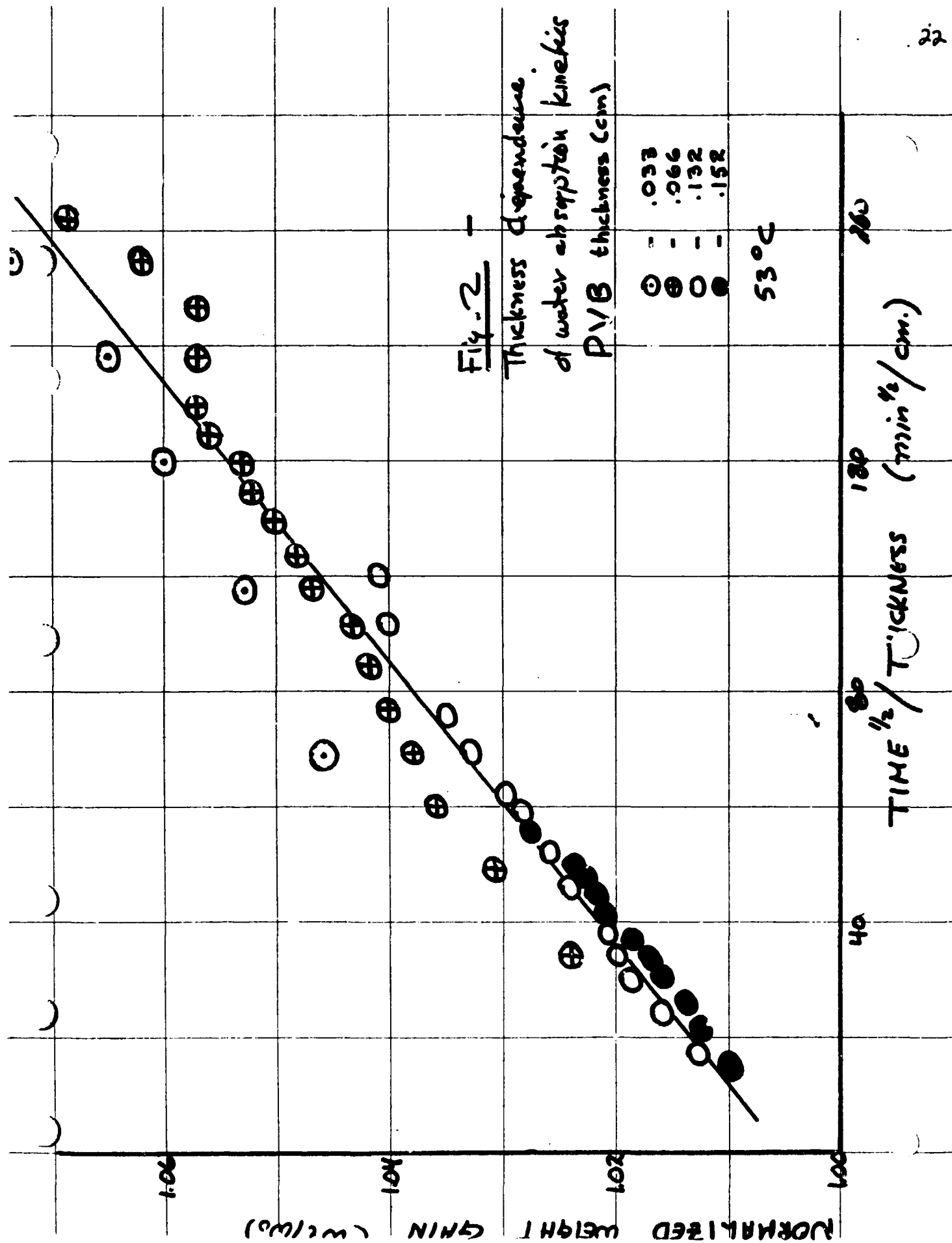
Future Work
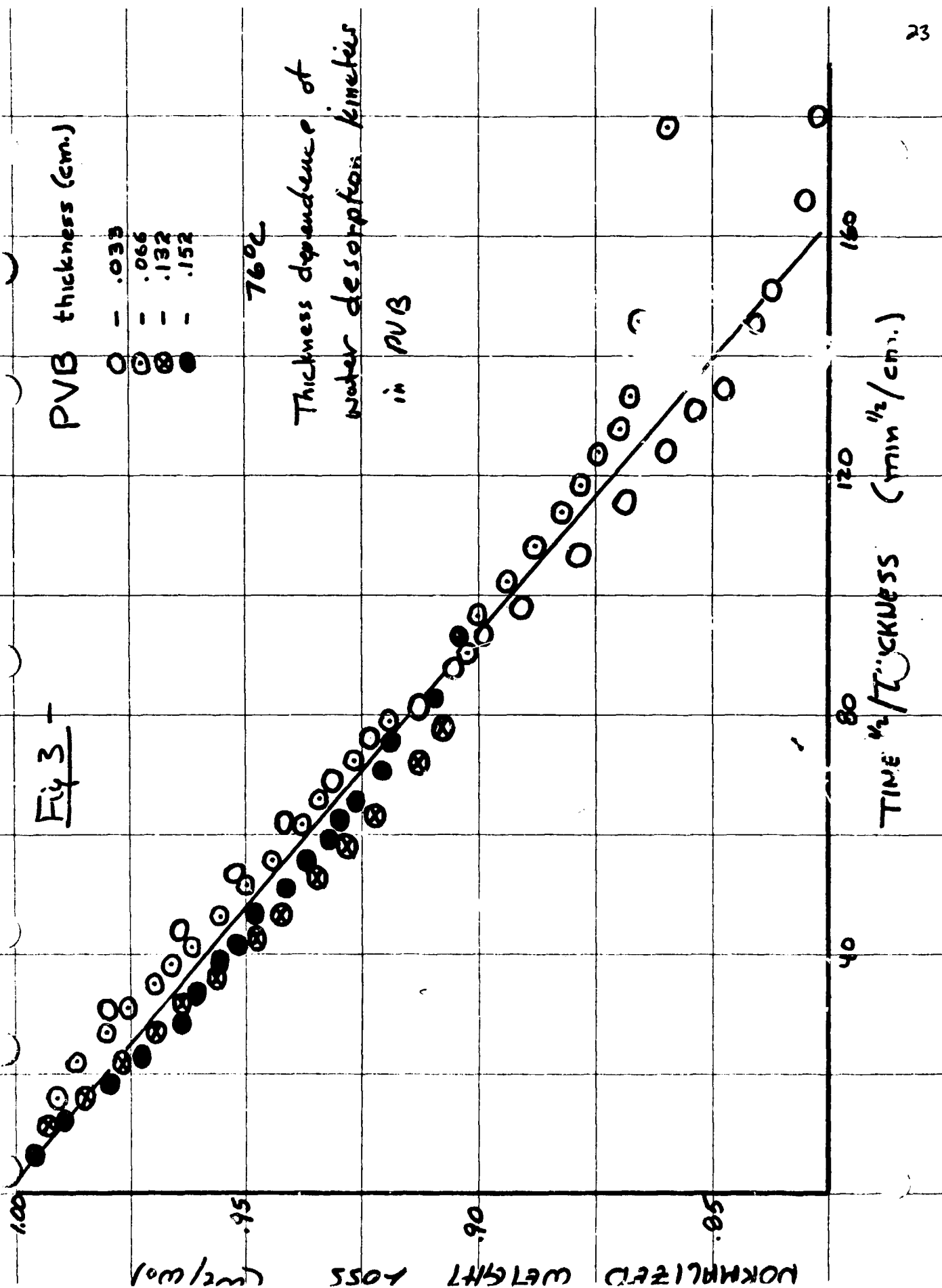
No future work is planned.

Fig—1
Water absorption
Kinetics in
PVB
at 53°C
— 0.152 cm Thick —

TIME (min)

TIME$^{1/2}$ (min$^{1/2}$)

FRACTIONALIZED WEIGHT (w_t / w_0)

1.03
1.02
1.01
1.00

0   20   40   60   80

2   4   6   8

21

Fig. 2

Thickness dependence
of water absorption kinetics

	PVB thickness (cm)
⊙	.033
⊕	.066
◯	.132
●	.158

53°C

NORMALIZED WEIGHT GAIN (wt/w₀)

TIME^½/THICKNESS (min^½/cm.)

22

Fig 3

PVB thickness (cm.)

○	—	.035
◐	—	.066
⊗	—	.132
●	—	.152

76°C

Thickness dependence of water desorption kinetics in PVB

NORMALIZED WEIGHT LOSS (gm/gm)

TIME $^{1/2}$/THICKNESS ($min^{1/2}$/cm.)

23

Fig 4 —

Water absorption kinetics (thickness dependence) in EVA; thickness (cm):

⊕ = .091
⊕ = .191
● = .248

53°C

NORMALIZED WEIGHT GAIN (wt/wo)

1.00   1.01   1.02   1.03

$TIME^{1/2}/THICKNESS$ ($mm^{1/2}/cm.$)

40   80   120   160
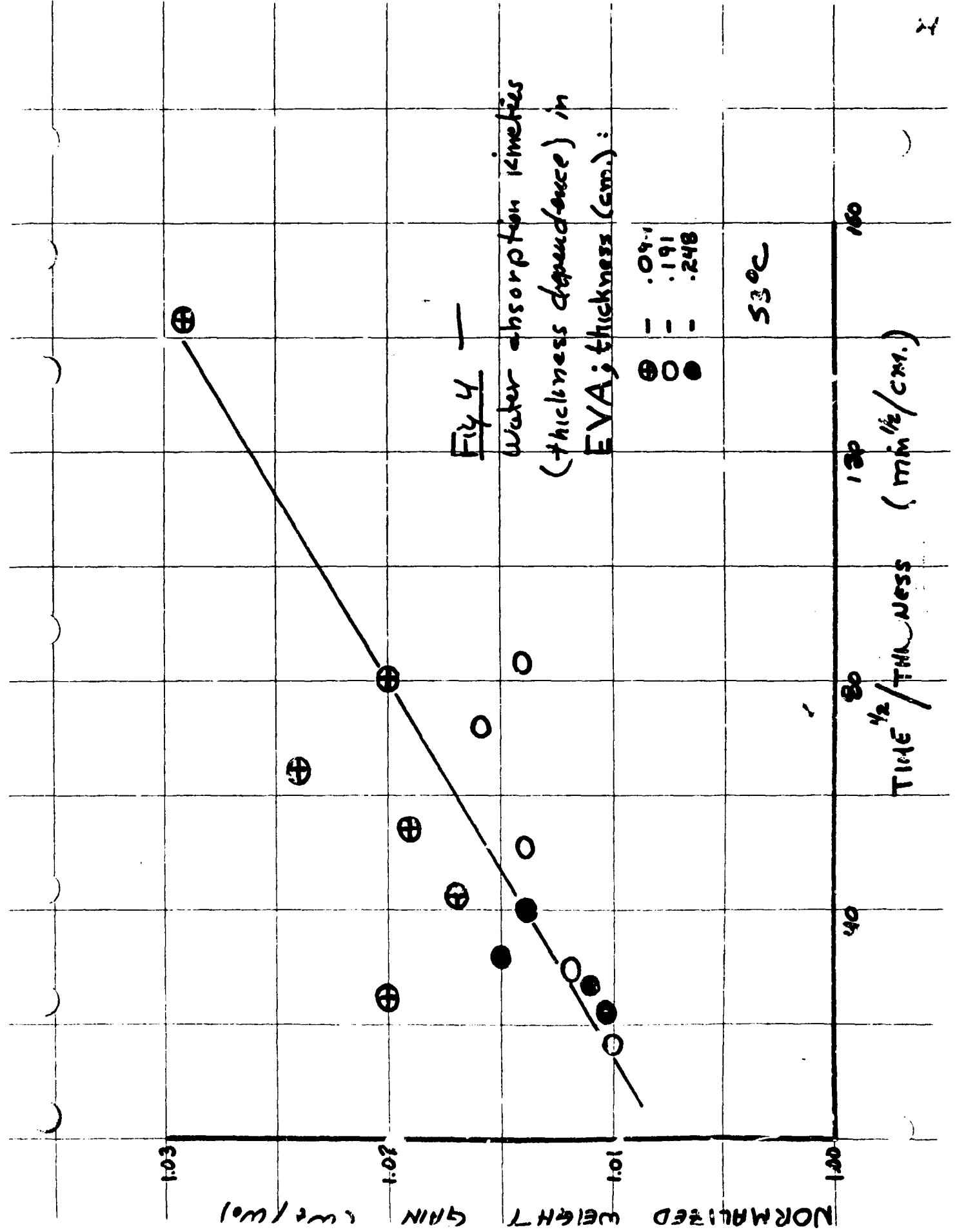
Fig 5 - Thickness dependence
of water desorption kinetics in
EVA - thickness (cm)

⊖ = .045
⊗ = .74
○ = .191
● = .284

76°C

NORMALIZED WEIGHT LOSS (wt/wo)

TIME ½ / THICKNESS (min½/cm.)

2.5
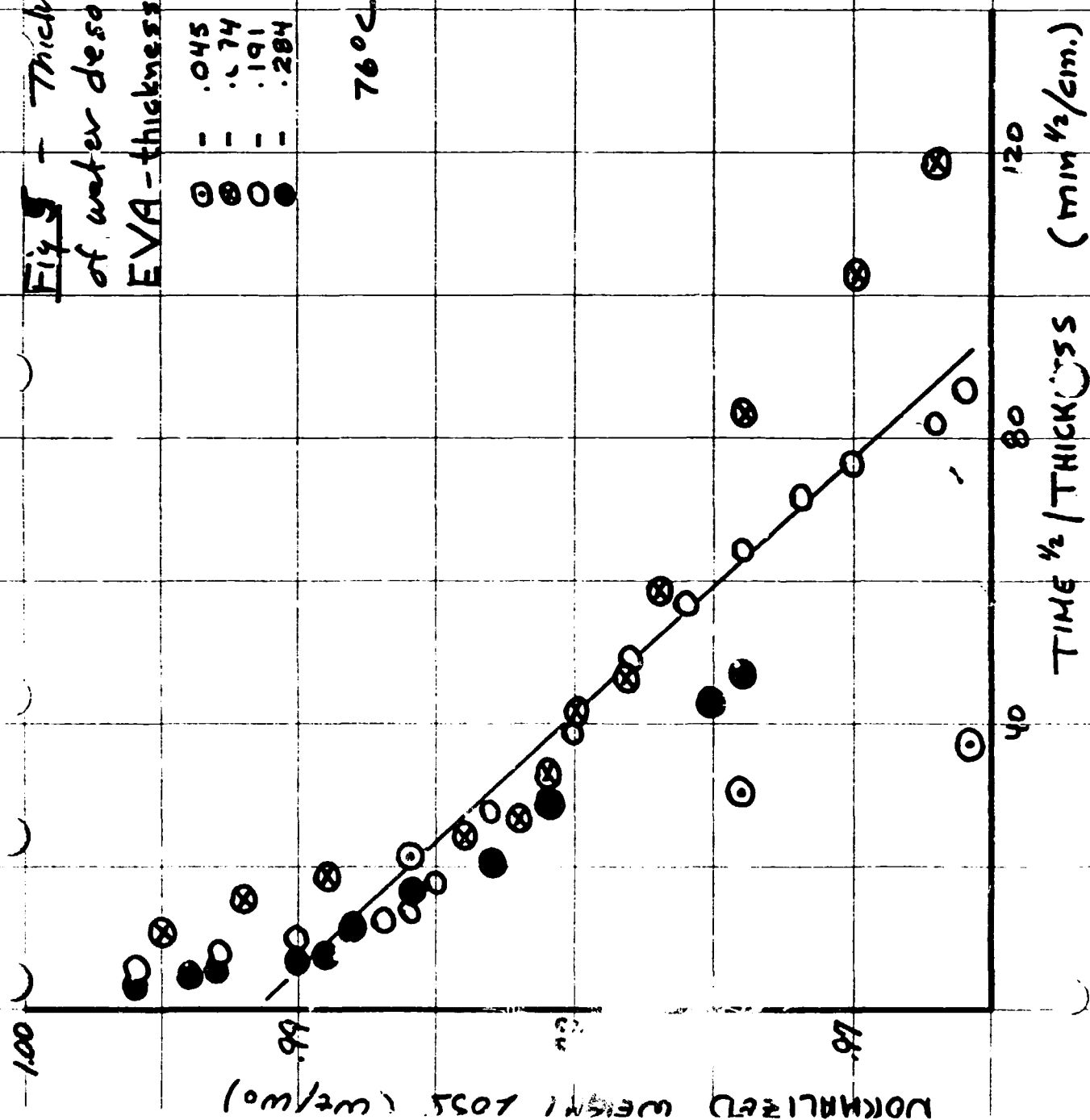
III. Corrosion Effects in Solar Cells

INTRODUCTION

In November, an attempt was made to separate the intercell
(potential difference) corrosion effect from the intracell
(dissimilar materials, galvanic action) corrosion effect in solar
cells and to evaluate the possibility of accelerated corrosion by
a photoelectrolysis effect in a polymer pottant containing water.
The experiments were arranged to address two questions:

(i) Is intercell potential difference or intracell
galvanic action more instrumental in causing
corrosion and the accompanying cell degradation
with service time.

(ii) Does a photoelectrolysis effect exist in the polymer
encapsulant of an illuminated solar cell and does the
effect accelerate corrosion and cell degradation in
much the same way that anodes for the photoelectrolysis
of water are degraded.

EXPERIMENTAL

The experiments consisted of encapsulating ASEC solar cells
in a PVB pottant. After encapsulation, the assemblies were immersed
in water to saturate the PVB. The testing procedure for evaluating
cell degradation due to corrosion consisted of measuring the I-V
characteristics curves of each encapsulated cell as a function
of immersion time in water for various testing arrangements
designed to evaluate intercell and intracell corrosion activity.
The first test arrangement (Cell #1) was an unbiased, nonilluminated,
short circuited single cell where any degradation of the original
I-V response curve as a function of immersion aging time would
result from the intracell corrosion effect alone. The second
test arrangement (Cell #2) was an unbiased, illuminated, short
circuited cell where any observed degradation of the original I-V
response curve is expected to be a measure of the combined effects of

both the intracell and the photoelectrolysis corrosion mechanisms.
The third test arrangement (cells #3 cathode and #4 anode) was
a coupled anode—cathode configuration where the cells were both
biased and illuminated. These encapsualted cells were coupled
by short circuiting their front side metallurgies and by connecting
a 5 volt biasing battery between their back side metallurgies.
No junction current due to the biasing battery is expected since
the #3 cathode cell was back biased in the coupling arrangement.
Any observed degradation of the original I-V response curves of
both the anode and cathode cells should then reflect the combined
effects of intercell, intracell and photoelectrolysis corrosion
mechanisms. By simply comparing the relative changes in the
I-V response curves of these four cells in these three testing
arrangements as a function of immersion time, the magnitudes of
the intercell, intracell, and photoelectrolysis degradation effects
can be separated and evaluated.

Results

A typical sequence of I-V response curves at various immersion
times is shown in Figure 1 for the #3 cathode cell. From these
curves for all four cells, the short circuit current (I_{sc}) and the
series (R_s) and shunt (R_{sh}) resistances were determined as a
function of immersion time.

The results for the short circuit current are presented in
Figure 2. For up to five days of testing, there appeared to be
no significant difference between the degradation of I_{sc} in
cell #1 (intracell), cell #2 (intracell and photoelectrolysis)
and cell #3 (cathode-intercell, intracell and photoelectrolysis).
On the basis of this observed feature, it was concluded that the

photoelectrolysis effect at the anti-reflection coating (assuming

its band gap energy exceeds 1.23 eV) has little or no influence

on solar cell degradation. After five days of testing, the

I_{sc} response of cell #4 (anode-intercell, intracell and photo-

electrolysis) was found to degrade the most (Figure 2).

After twenty days of testing, the degradation of I_{sc} in

both the cathode and anode cells are about equal and significantly

larger than the I_{sc} degradation in cell #2 (Figure 2). Assuming

that the photoelectrolysis effect is absent, the intercell and

intracell effects can be separated by comparing the results for

cell #2 with cells #3 and #4. For twenty hours of testing, this

separation is shown on Figure 2 where it is apparent that the

degradation of I_{sc} due to intercell corrosion appears to be

about equal in magnitude to that due to intracell corrosion.

Since the applied potential difference between the two cells in

this study is small compared with potential differences

frequently occurring between adjacent cells in module mounted

arrays, the intercell corrosion effect is expected to have a

significantly larger influence on degrading solar cell activity

than the intracell corrosion effect resulting from the composite

material structure (Ti, Ag, Pd, A/R Si) associated with each

cell. The surprising feature of the data after twenty days, is

that I_{sc} for the cathodic cell degraded as much as for the anodic

cell.

The time dependence of R_s and R_{sh} can also be evaluated from

the I-V curves for each cell in the various testing arrangements.

A comparison of R_s as a function of time for the anodic and

cathodic cells is presented in Figure 3. The series resistance

for the anodic cell increases continuously with time while R_s for the cathodic cell remains relatively time independent for time values less than ten days. After ten days, R_s of the cathode cell increases rapidly.

The continuous increase of R_s with time for the anodic cell can be justified from simple considerations. As a first approximation, the series resistance would by given by

$$R_s = \rho_c \ell_c / A_c \tag{1}$$

or

$$dR_s = -\left[\rho_c \ell_c / A_c^2\right] dA_c \tag{2}$$

where ρ_c is the composite resistivity of the front side metallization, ℓ_c is its effective length and A_c is its cross sectional area. Faraday's law suggests that electrochemical corrosion at the anode will decrease the cross sectional area at a constant rate (K):

$$dA_c / dt = - K \tag{3}$$

so

$$dR_s \simeq \left[\rho_c \ell_c / A_c^2\right] K \, dt \tag{4}$$

or

$$R_s \sim t \tag{5}$$

This predicted continuous increase in R_s with time is evident in the anode date shown in Figure 31.

The observed time dependence for the R_s data of the cathode can also be justified by simple considerations. Electrochemcial plating occurs at the cathode. The series resistance could then be given approximately by

$$\frac{1}{R_s} = \frac{1}{R_c} + \frac{1}{R_f} = \frac{A_c}{\rho_c \ell_c} + \frac{A_f}{\rho_f \ell_f} \tag{6}$$

where ρ_f, ℓ_f and A_f are the resistivity, effective length and cross sectional area of the plated film. The cross sectional

area of the plated film is proportional to its thickness (X_f):

$$A_f \sim X_f \qquad (7)$$

and X_f for a simple plating operation is directly proportional to the time:

$$X_f \sim t \qquad (8)$$

The series resistance for the cathode cell from Equation 6 would then involve a composite resistance term (R_c).

$$R_c = f_c \ell_c / A_c \neq fct(t) \qquad (9)$$

which is time independent and a plated film resistance term R_f

$$R_f = f_f \ell_f / A_f = fct(t) \qquad (10)$$

which is time dependent. Initially when the plated thickness is thin,

$$R_c < R_f \qquad (11)$$

and the series resistance will simply be equal to the time independent composite resistance term

$$R_s \simeq R_c \qquad (12)$$

The experimental data support this conclusion in that R_s for the cathode cell is independent of time when time is less than 5 days (Fig. 3). At longer immersion time values when X_f is not thin

$$R_f < R_c \qquad (13)$$

and the series resistance becomes linearly time dependent:

$$R_s \simeq R_f = K_1 t \qquad (14)$$

This predicted feature is also evident in the experimental data of the cathode cell (Fig. 3) for time values in excess of five days.

The series resistance of cell #2 monitoring intracell corrosion effects as a function of time, is shown in Figure 4, and is seen to be much less time dependent that was evident in the anodic or cathodic cell results (Fig. 3). This comparative feature supports the previous suggestion that intercell corrosion is more influencial than intracell corrosion in causing solar cell degradation.

The behavior of the shunt resistance as a function of time for the cells is presented in Figures 5 and 6. The shunt resistance of the cathodic cell decreases continuously and rapidly with time (Fig. 5) while R_{sh} for the anodic cell remains time independent until about five days have elapsed, and then decreases rapidly with time (Fig. 5). The time dependence of R_{sh} for cell #2, is shown in Figure 6, and is almost identical to the functional response seen in Figure 5 for the anodic cell. This similarity suggests that only the intracell corrosion effect is governing the R_{sh} behavior of the anodic cell.

Simple intercell plating considerations can be used to explain the time dependence of R_{sh} in the cathodic cell. The continuous decrease in R_{sh} with time in the cathodic cell shown in Figure 5, will result when plating occurs on a cell edge. This plated film effectively shorts the front side metallization to the back side metals with a film that gets progressively thicker (less resistive) with increasing time as suggested by Equation 8.

Simple intercell corrosion considerations would suggest that R_{sh} for the anodic cell should remain large, and not degrade with time. This feature is evident in Figure 5 for the anode for

time values less than five days. For time values greater than five
days, intracell corrosion effects becomes evident as suggested
previously, and this effect decreases the shunt resistance by a
mechanism that is not clear. Several possible mechanisms are
intracell plating, and dendrite formation.

These simplified plating concepts that were used to explain the
behavior of R_{sh} and R_s as a function of time in the cathodic cell
can also be used to show that I_{sc} should decrease with time in the
cathodic cell. The thin plated film decreases the intensity of
the light being transmitted through the film into the solar cell
by an amount that is governed by the absorption law for a plated
film of thickness x:

$$P_s \sim exp(-\alpha x_f) \qquad (15)$$

where α is the absorption coefficient and P_s is the intensity of
the light transmitted into the cell. SInce I_{sc} is directly propor-
tional to P_s

$$I_{sc} \sim P_s \qquad (16)$$

then the short circuit current becomes

$$I_{sc} \sim exp(-\alpha x_f) \qquad (17)$$

or from Equation 8

$$I_{sc} \sim exp(-k_2 t) \qquad (18)$$

showing that the short circuit current decreases with time for
the cathode cell as is evident in Figure 2 which shows a linear
decrease even though Equation 18 predicts an exponential decrease.

<div align="center">CONCLUSIONS</div>

·Cell degradation by photoelectrolysis is not
apparent in polymer (water saturated) encapsulated
solar cells.

·Intracell corrosion due to dissimilar materials is
not expected to be as important as intercell
corrosion due to potential differences in solar
cell arrays.

·Very simple plating and corrosion concepts can be used to predict the time dependency for the degradation of R_s, R_{sh}, and I_{sc}. for cathodic and anodic solar cells. The predicted dependencies were in reasonable accord with the experimental data.
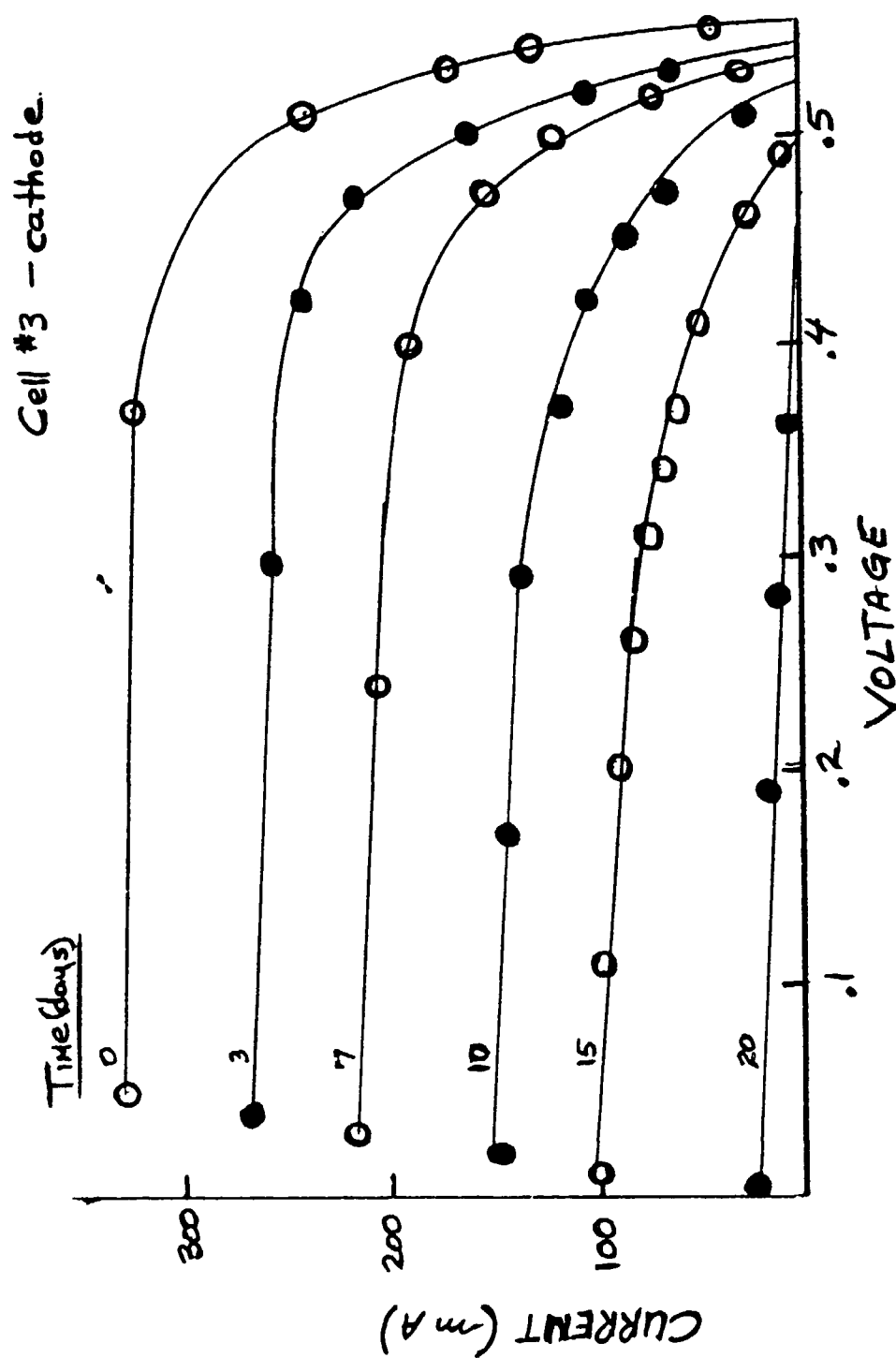
Future Work

No future work.

Figure 1 — Characteristic current-voltage response curves of a cathodically polarized, PVB encapsulated solar cell for various aging times.
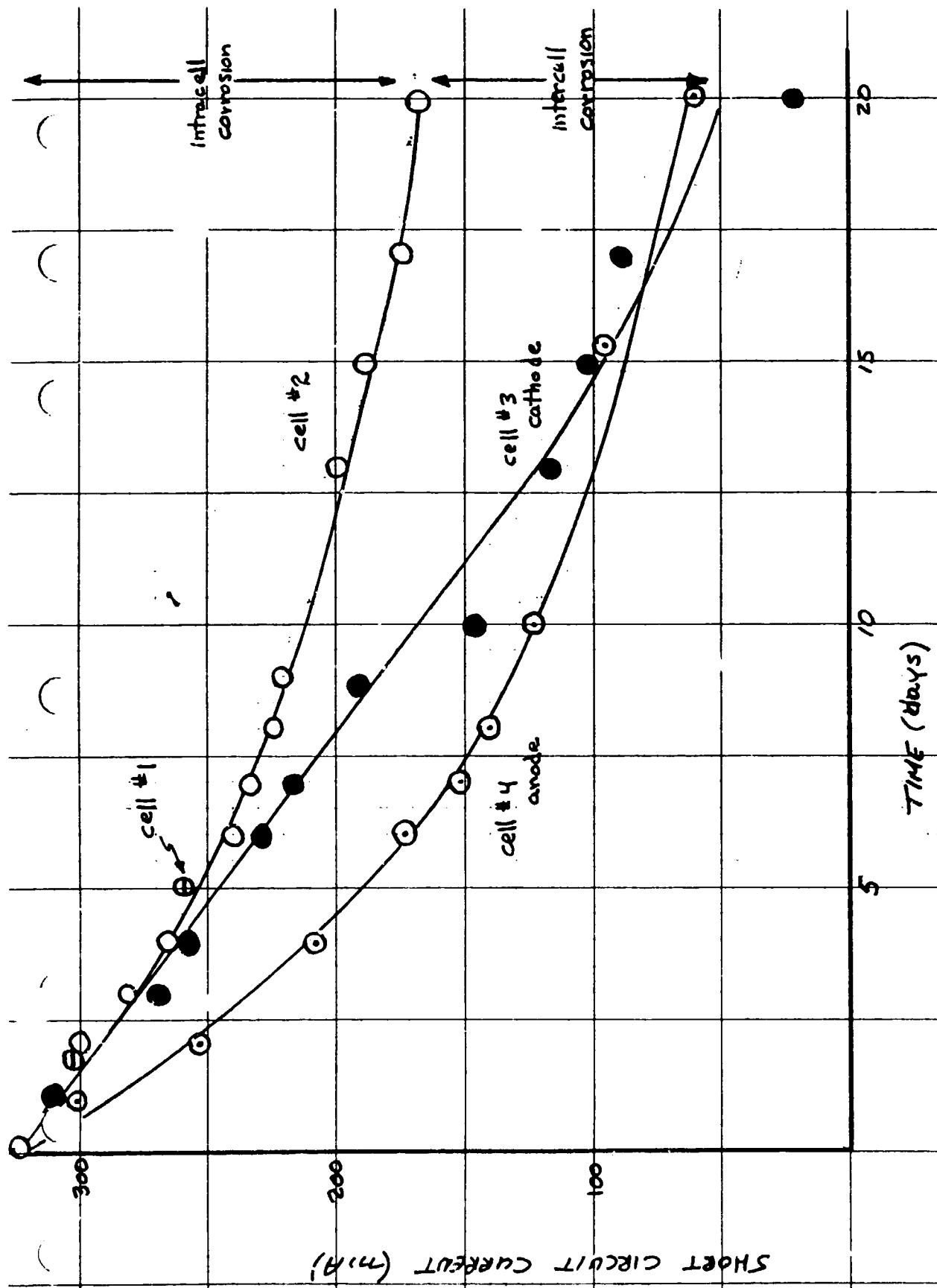
Figure 2 — Short circuit current as a function of aging time for PVB encapsulated solar cells representing: intracell corrosion (cell #1); intracell and photoelectrolyis corrosion (cell #2); and intracell, photoelectrolysis, and intercell corrosion (cell #3 -cathodically polarized and cell #4-anodically polarized)

Figure 3 —

Series resistance as a function of aging time for PVB encapsulated solar cells experiencing intercell and intracell corrosion effects in cathodic polarization (cell #3) and in anodic polarization (cell #4).
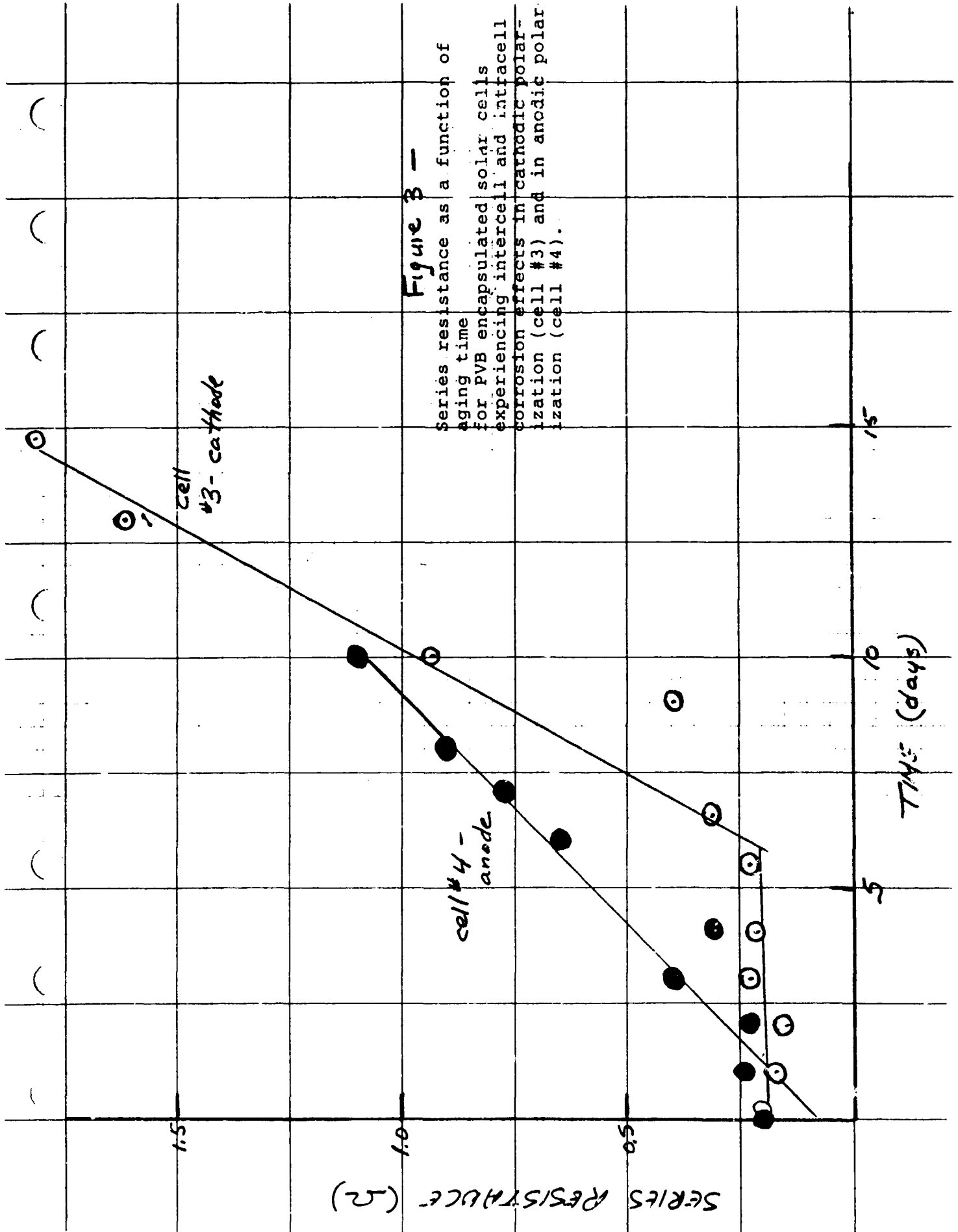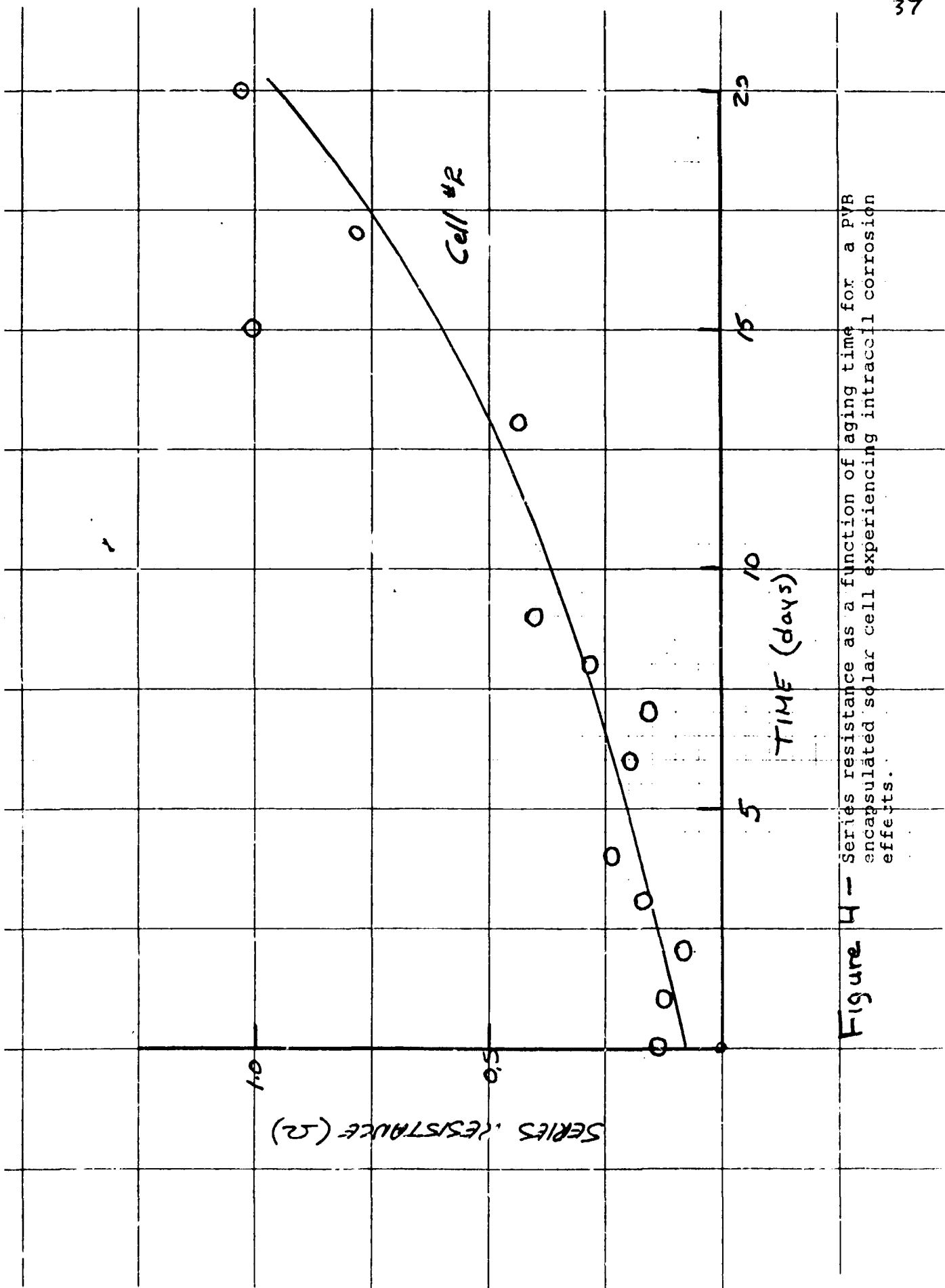
Figure 4 — Series resistance as a function of aging time for a PVB encapsulated solar cell experiencing intracell corrosion effects.
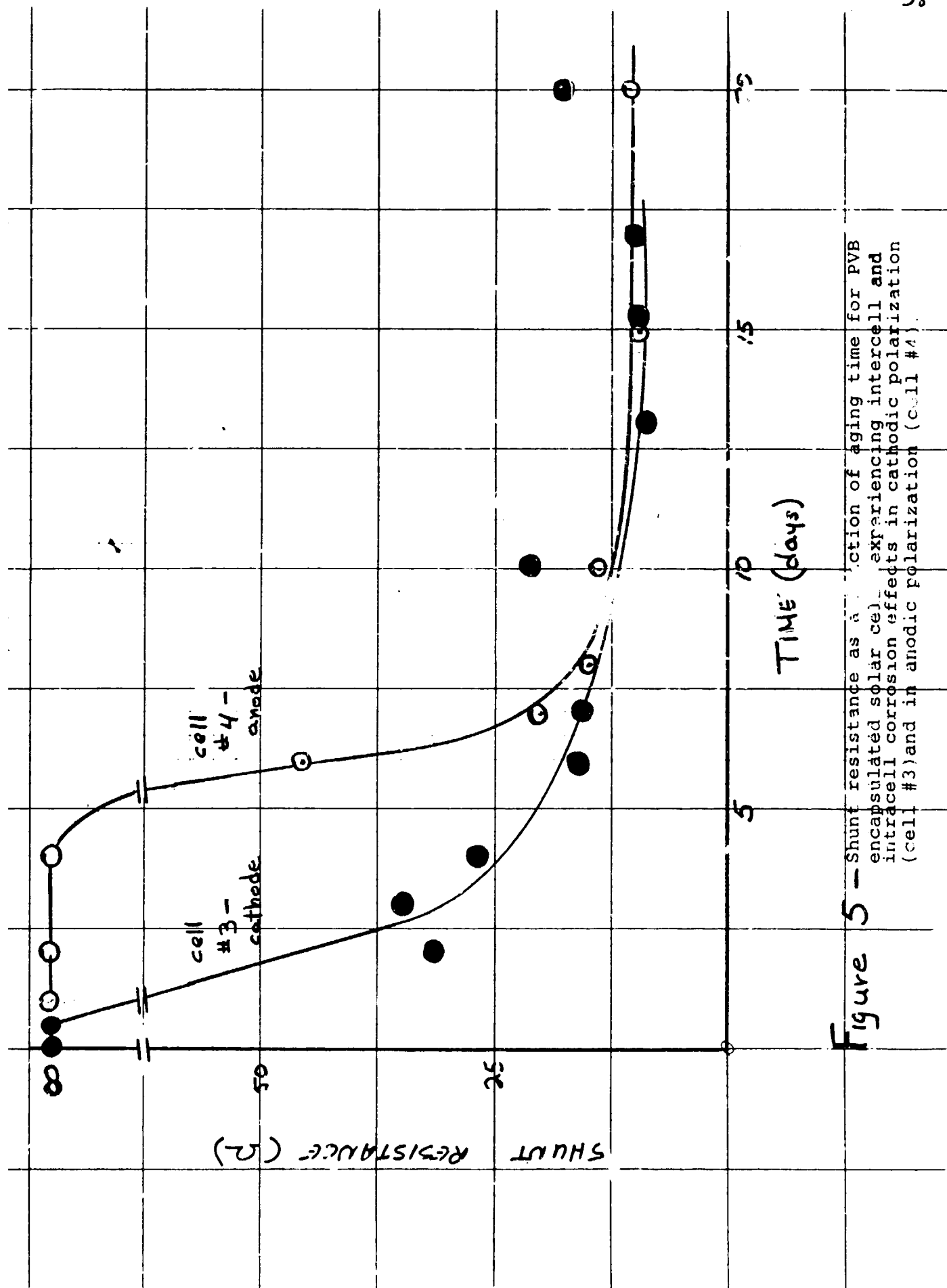
Figure 5 — Shunt resistance as a ... ction of aging time for PVB
encapsulated solar cell exeriencing intercell and
intracell corrosion effects in cathodic polarization
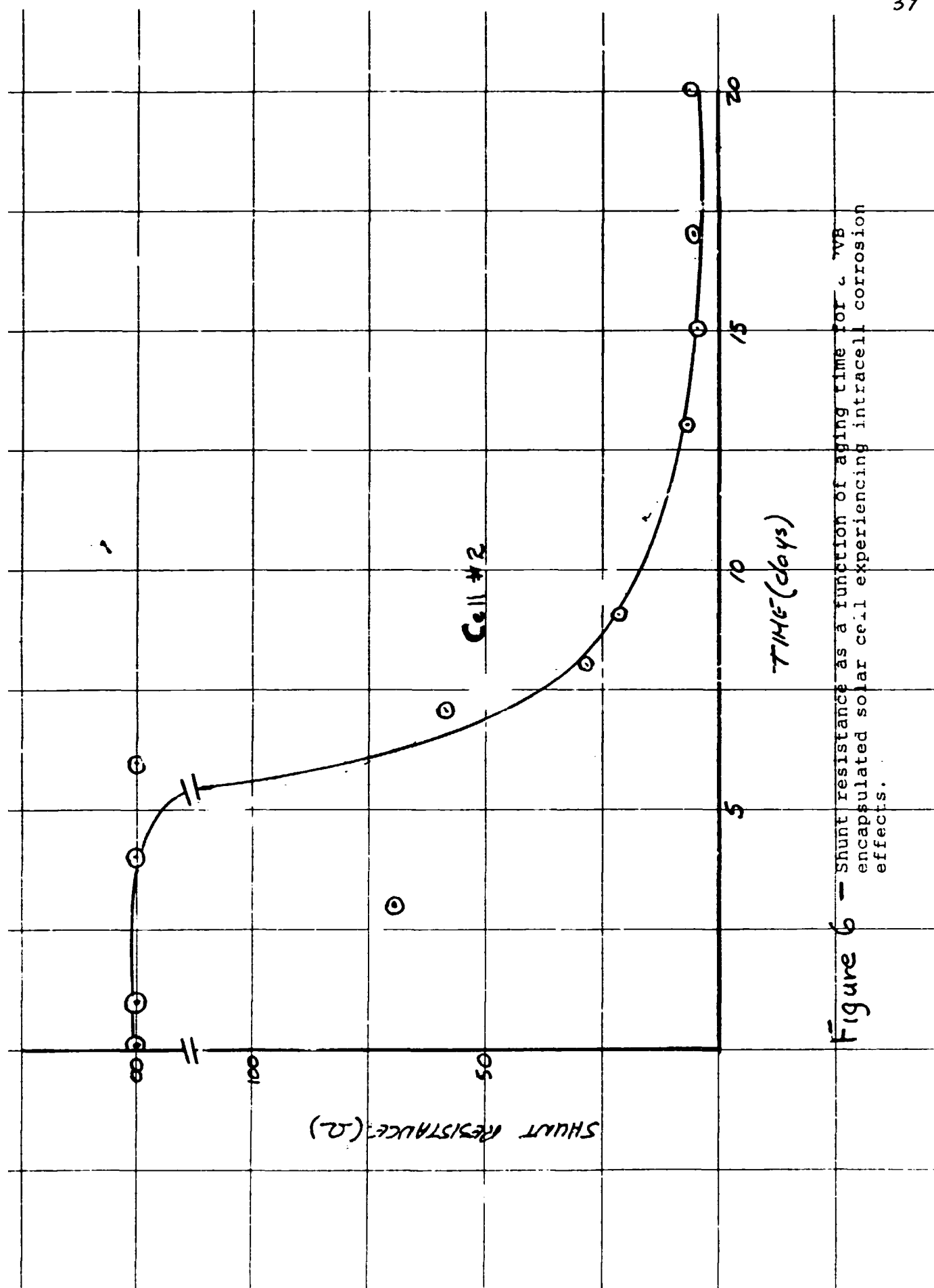(cell #3) and in anodic polarization (cell #4).

Figure 6 — Shunt resistance as a function of aging time for a VB encapsulated solar cell experiencing intracell corrosion effects.